Palaeogeography, Palaeoclimatology, Palaeoecology 542 (2020) 109585

Contents lists available at ScienceDirect

Palaeogeography, Palaeoclimatology, Palaeoecology

journal homepage: www.elsevier.com/locate/palaeo

A transient simulation of precession-scale spring dust activity over northern China and its relation to mid-latitude atmospheric circulation

Xinzhou Li[a,b,*], Xiaodong Liu[a,b], Zaitao Pan[c,d], Zhengguo Shi[a], Xiaoning Xie[a], Qingchun Guo[e]

[a] State Key Laboratory of Loess and Quaternary Geology, Institute of Earth Environment, Chinese Academy of Sciences, Xi'an, China
[b] CAS Center for Excellence in Tibetan Plateau Earth Sciences, Beijing, China
[c] Department of Earth and Atmospheric Sciences, Saint Louis University, St. Louis, MO, USA
[d] Key Laboratory of Meteorological Disaster, Ministry of Education, Nanjing University of Information Science and Technology, Nanjing, Jiangsu, China
[e] School of Environment and Planning, Liaocheng University, Liaocheng, Shandong, China

ARTICLE INFO

Keywords:
Asian dust
Westerly Jet
Precessional cycle
Tibetan Plateau
Surface heating
Siberian high

ABSTRACT

Dust aerosol plays an important role in energy and water cycles of the earth system across multiple spatial and temporal scales, and it is also a key factor in determining air quality in arid and semi-arid areas of Asia. Spring is the season of peak dust activity (i.e. emission, transport, and sedimentation) in Asia. However, on the Earth's orbit scale, spring dust activity in northern China (NC) and its relationship with atmospheric circulation have seldom been investigated. We present the results of an analysis of the evolution characteristic on the astronomical timescale, and dynamic mechanism of spring dust activity in NC, based on a transient numerical simulation over the past 150 kyr spanning multiple precessional cycles. We found that within the precessional band, spring dust transport is in-phase with insolation, the upper Westerly Jet on the north (nWJ) of the Tibetan Plateau (TP), surface wind, and heating of the TP; whereas it is out-of-phase with Siberian high (SH), atmospheric precipitation, and soil water. During the high-insolation stage, the nWJ is strengthened by the thermal forcing of the TP, which causes a northward shift of the location of the Westerly Jet, so that dust activity is enhanced by the propagation of upper-level waves. Meanwhile, during the high-insolation stage, the instability of the lower atmosphere is increased due to the strengthening of the northerly wind associated with the weakening of the SH and surface warming, together with their higher interaction, with the nWJ giving rise to dust mobilization in the Asian arid and semi-arid source areas, and vice versa. Rainfall and soil moisture have little influence on the dust cycle on the orbital scale, although modern observations show they have an important inhibitory effect on dust emission.

1. Introduction

Dust aerosol plays an important role in energy and water cycles of the earth system by linking radiation, precipitation, and atmospheric circulation on multiple temporal and spatial scales. Many observational and modeling studies on Asian dust cycle have been documented (e.g., Zhang et al., 1997; Zhao et al., 2006; Uno et al., 2009). Dust activity (i.e. emission, transport and sedimentation) in East Asia is the strongest in spring (Liu et al., 2004; Roe, 2009), possibly because intense dust activity requires the simultaneous operation of three factors: the long duration of the strong winds, abundance of dust particles, and instability of the atmospheric stratification. The Asian dust source region is relatively constant geographically, and hence wind speed and the stability of the atmosphere are the key factors determining the dynamics of dust activity. As solar heating develops during the day, the atmosphere often becomes unstable towards afternoon, leaving the strong winds as the main factor in determining sandstorm occurrence.

The Eurasian interior contains the most extensive arid and semiarid areas on Earth (Han et al., 2014). The Taklimakan Desert, Mu Us Desert, Badain Jaran Desert, Tengger Desert, and the vast Gobi Desert in northern China (NC) are the main dust source areas of Asian arid region (Fig. 1), and the dust hazards have become a key factor determining air quality. With recent advances in high-resolution modeling and the increasing availability of long-term geological records, there is increasing evidence indicating that the climate of Eurasian on orbital timescales is directly controlled by insolation. The long loess and paleosol sequences from the Chinese loess Plateau (CLP) show that dust activity exhibits significant orbital periodicities (Li et al., 2015). Using grain-size records of the last glacial cycle from CLP, Sun (2004) suggested that the strength of the westerly circulation and winter monsoon over East Asia

* Corresponding author at: Institute of Earth Environment, Chinese Academy of Sciences, 97, Yanxiang Road, Xi'an, Shaanxi 710061, China.
E-mail address: lixz@ieecas.cn (X. Li).

https://doi.org/10.1016/j.palaeo.2020.109585
Received 15 August 2019; Received in revised form 3 January 2020; Accepted 3 January 2020
Available online 07 January 2020
0031-0182/

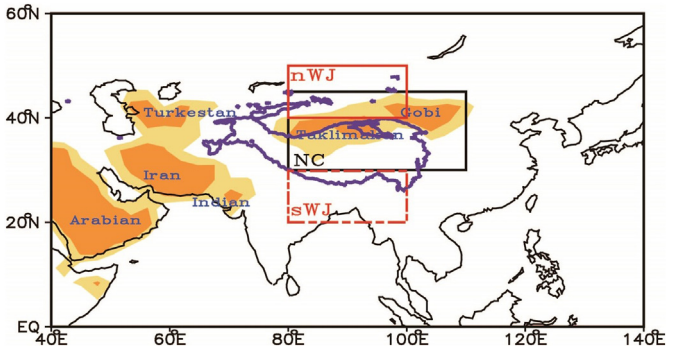

Fig. 1. Distribution of desert regions in Asia (shaded) and the regions of interests in this study. NC: northern China (80–110°E, 30–45°N, black solid box); nWJ: active area of the Westerly Jet on the north side of TP (80–100°E, 40–50°N, red solid box); sWJ: active area of the Westerly Jet on the south side of TP (80–100°E, 20–30°N, red dashed box). The purple contour delineates the distribution of TP terrain > 3-km elevation. (For interpretation of the references to colour in this figure legend, the reader is referred to the web version of this article.)

were synchronously intensified during glacial stages and weakened during interglacial stages. In addition, loess records from Central Asia (Ding et al., 2002) and aeolian sedimentary records from the Japan Sea (Nagashima et al., 2007) have revealed significant variations of Asian dust activity on the orbital scale and their close relationships with atmospheric circulation. Other geological records, such as from stalagmites (Bar-matthews et al., 2003; Yuan et al., 2004; Wang et al., 2008a, 2008b; Cheng et al., 2012) and marine sediments (Wang et al., 2005), also indicated that the regional climate of Eurasia experienced pronounced cyclicity on the orbital cycles. Numerous numerical experiments, including time-slice equilibrium simulations (Kutzbach, 1981; Prell and Kutzbach, 1987) and continuous transient simulations (Kutzbach et al., 2008; Li et al., 2013; Wang et al., 2016), have confirmed the prominent orbital-scale cyclicity of Asian climates. However, the precise mechanism of East Asian dust activity on the Earth-orbital scale are still not fully understood.

The upper tropospheric mid-latitude westerly in the Northern Hemisphere (NH), as an important component of the atmospheric circulation, plays a key role in determining the weather and climate of Asia, and it therefore affects the dust cycle over the arid areas of Asia on multiple timescales (Li et al., 2019). The intensity and location of the Westerly Jet axis (WJL) exhibit a pronounced seasonal evolution (Zhang et al., 2006; Schiemann et al., 2009), and they have a major influence on the Asian climate change and on dust cycle throughout the troposphere (Jia et al., 2018), all year-round. As an elevated heat source, the TP has exerted an important influence on the westerly and its seasonal variation (Schiemann et al., 2009; Chiang et al., 2015; Li and Liu, 2015b; Li et al., 2017; Zhang et al., 2017). In spring, as the surface heating of the TP intensifies, the weakening zonal flow above the TP tends to cause a latitudinal shift of the Westerly Jet or splitting between northern (nWJ) and southern (sWJ) sides of the TP (Fig. 1). The seasonal migration and variation of the intensity of the Westerly Jet largely control the weather, climate and dust activity in mid-latitudes Asia (Kohfeld et al., 2013; Chang et al., 2002; Li and Liu, 2015b). Notably, Li and Liu (2015b) found that the westerly around the TP is the most unstable in term of latitudinal position in spring, which is the season of peak dust activity in NC. In addition, the SH is much weaker in spring, resulting in the instability of lower atmosphere which promotes increased dust activity (Roe, 2009). Unlike glacial periods when high northern latitudes were covered by ice sheets (Anderson et al., 1988; Pinot et al., 1999), during interglacials the insolation changes caused by Earth's orbital cyclicity was the main driver of climate change. However, relatively little research has been conducted on the evolution of Asian dust activity on the orbital scale, and on the dynamical mechanism associated with atmospheric circulation and insolation. In the present study, we conducted a long-term transient simulation in which Earth orbital forcing alone was used to analyze the shifts of the Westerly Jet and their interaction with lower atmospheric circulation. Our aim was to explore the dynamic mechanism of dust activity within the precessional band.

The rest of this paper is organized as follows. Briefly describing observational and reanalysis data, the model used, and experimental design are presented in Section 2. In Section 3, we analyze the long-term evolution of dust activity and relevant climatic elements within the precessional band. In Section 4, we attempt to explain the relationships between the Westerly Jet and its latitudinal shifts, SH, TP heating, surface wind, vertical circulation, and dust activity, based on analyses of high and low insolation stages. The major discussion and conclusions are presented in Sections 5 and 6, respectively.

2. The data and model

2.1. Reanalysis and observational data

Two reanalysis datasets were used to analyze the relationship between modern dust activity and atmospheric circulation and to verify the numerical simulation results. The first is the dust emission flux data from the Modern-Era Retrospective Analysis for Research and Applications, version 2 (MERRA2) dataset (Gelaro et al., 2017) produced by NASA's Global Modeling and Assimilation Office. MERRA2 includes hourly to monthly mean dust emission flux, dust column mass density, dust surface mass concentration, dust column horizontal mass flux, and dust sedimentation flux, at a spatial resolution of longitude 0.625° × latitude 0.5° for 1980–2016 (Buchard et al., 2017; Liu et al., 2018). The average dust emission flux in spring during 1980–2016 is shown in Fig. 2a. The other dataset is the National Centre for Environmental Prediction (NCEP) reanalysis for 1954–2007. The NCEP reanalysis data are the combination of the medium range forecast (MRF) T62 model hindcast with in-situ observations (Kalnay et al., 1996). The reanalysis data have a horizontal resolution of 2.5° × 2.5°

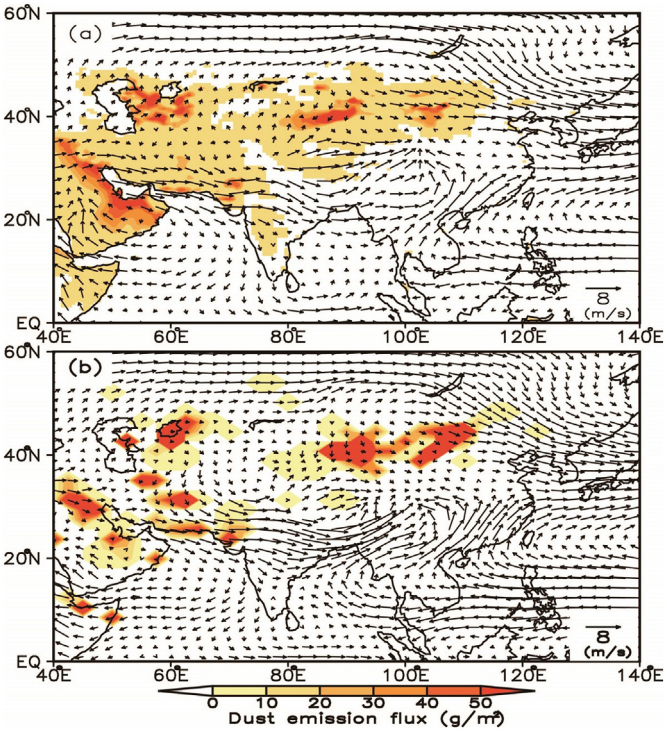

Fig. 2. Dust emission flux (colour shaded, unit: g/m^2) and the 850 hPa wind vector field (m/s) in spring. (a) MERRA2 and NCEP; (b) CESM1.2.

and 17 vertically layers from 1000 to 10 hPa. The variables used in this study of the NCEP reanalysis data are surface temperature, surface sensible heat flux and winds.

Observational data of sandstorms were obtained from the China Meteorological Information Center (http://data.cma.cn/). Each sandstorm event (visibility < 1 km) was carefully recorded (Liu et al., 2013) and the dataset quality was controlled with a high degree of consistency (Zhou and Zhang, 2003). This dataset includes the start and end times of each dust storm, visibility, and the wind speed. We selected observational data on dust storms at 181 sites in NC covering the common period of 54 years (1954–2007). The station–hour is used to represent the intensity of a sandstorm; that is, the duration of sandstorm in hours (Li and Liu, 2015a). This enabled us to obtain sequences of observed strong sandstorms that link the dust activity in NC and variability of the WJ.

2.2. Numerical model and experimental design

Version 1.2 of the Community Earth System Model (CESM1.2) of the National Center for Atmospheric Research was used in this study. CESM1.2 is a fully coupled global climate model consisting of five components: the atmosphere (the Community Climate System Model, CAM), the land (the Community Land Model, CLM), the ocean (the Parallel Ocean Program, POP), the sea ice (the Sea-Ice Component, CICE) and the Coupler. It is currently one of the world's most advanced air-sea-land coupled models (Hurrell et al., 2013). The versions of each component are respectively CAM5, CLM4, POP2, CICE4, CPL6. The horizontal resolutions of the CAM5 and CLM4 are ~1.9° × 2.5° and the vertical dimension contains 30 and 15 levels, respectively. The ocean and sea ice components have a horizontal resolution of 1° × 1° and depth (z) coordinates of 40 levels.

Notably, CAM5 in CESM1.2 incorporated a dust aerosol module parameterizing dust emission, transport, and deposition (Neale et al., 2010). The generation of dust particles is calculated based on the Dust Entrainment and Deposition Module (Zender et al., 2003). The simulation of the dust cycle in CAM5 was described and validated with observational data (Mahowald et al., 2006; Yoshioka et al., 2007; Li et al., 2016). Li et al. (2016) compared the atmospheric circulation, dust emission fluxes, and dust optical depth from CESM1.2 with NCEP reanalysis and Multi-angle Imaging Spectro-radiometer (MISR, http://www-misr.jpl.nasa.gov) data. The results showed that the CESM1.2 and dust modules can effectively simulate dust activity. The spatial distribution of spring dust emission flux averaged from MERRA2 and the 850 hPa wind field averaged for 1980–2010 from NCEP reanalysis, are shown in Fig. 2a. It is evident that the dust emission flux was greatest ($> 50\ g/m^2$) over the dust source regions of central Asia and northwest China (Fig. 1). Similarly, the dust emission flux and the 850 hPa wind field averaged for 1980–2010 derived from a 20th-century transient (1850–2005) using CESM1.2 are illustrated in Fig. 2b. The horizontal distribution of dust emission and the wind field from CESM1.2 resemble the observations quite well, although the model overestimates the amplitude of dust emission flux. The bias is probably due to the model's coarse horizontal resolution and soil erosion factors. Overall, CESM1.2 can reliably capture the characteristics of dust activity and atmospheric circulation.

Using CESM1.2, we conducted a long-term transient experiment starting at 150 kyr BP using the orbital acceleration technique (Jackson and Broccoli, 2003; Lorenz and Lohmann, 2004). The simulation was started using fixed orbital parameters at 150 kyr BP to generate a quasi-equilibrium state for the first 100 years, which is completely satisfied when only changing the solar radiation. In this study, CESM1.2 used an acceleration factor of 100 (1 model year = 100 calendar years), similarly to the previous experiments using CCSM3 (Li et al., 2013). Thus, the output 1500 model years represent the period from 150 kyr BP to the present. In CESM1.2, a three-dimensional dynamic ocean (POP2) is used to ensure a reasonable surface sea temperature (SST), although the deeper seawater temperature is not realistic in the transient simulation (Kutzbach et al., 2008). To highlight orbital irradiance effects alone, the experiment does not consider changes in other factors such as surface vegetation coverage, greenhouse gases, and high latitude glacial sheets. The atmospheric CO_2, CH_4 and N_2O concentrations are held constant at 289 ppm, 901 ppb and 281 ppb, respectively, as well as their pre-industrial values. During the entire integration, all boundary conditions remain fixed to present day, except for Earth orbital forcing (Li et al., 2013). All three orbital parameters (eccentricity, obliquity, and precession) are allowed to vary simultaneously during the course of the integration.

In order to fully demonstrate the effects of Earth orbital-scale insolation, we choose the highest insolation stage (centered at ~129.3 ± 0.5 kyr BP, a total of 1100 calendar years and referred to as the HI period) and the lowest insolation stage (centered at ~118.1 ± 0.5 kyr BP and referred to as the LI period) in order to further explore how HI and LI insolation affects the TP heat source, WJ, SH, surface wind, and dust activity in NC. The simulated long-term time series were smoothed by a 3-kyr moving averages (30 model years) for improved graphical clarity and to aid interpretation.

3. Long-term evolution of dust activity and relevant climatic elements

3.1. Dust activity and geological record

Long time-series of dust activity derived from numerical simulations and their comparison with high-resolution geological records can provide an improved understanding of the history of dust activity within the Asian interior and its possible dynamic relationships with multiple natural factors. This section presents the evolution of model-simulated spring dust emission and deposition in NC during the last 150 kyr. The dust emission (DE-NC, averaged for 80–110°E, 30–45°N) and deposition (DD-NC) fluxes in NC comprise six complete 20-kyr cycles and are synchronized closely with cyclicity of NH spring insolation (Fig. 3a and d). During a precessional cycle, dust activity in NC gradually strengthens (weakens) as solar radiation increases (decreases). Unlike the symmetric insolation cycle, dust emission and deposition cycles are slightly asymmetrical, with the rising phase increasing slightly faster than descending phase (similar to temperature cycle at the eccentricity scale: Petit et al., 1999).

High resolution loess sequences from the CLP demonstrate the high sensitivity of Asian dust activity and monsoon variability to changing insolation and glacial boundary conditions (Sun et al., 2015). We present a loess time series of mean grain size (MGS) (Fig. 3b) at Gulang (37°28′43″N, 102°52′28″E), located in the northwestern CLP, and compare it with the simulated dust flux during the last 150 kyr. The MGS record exhibits an obvious 100-kyr ice-age cycle associated with glacial forcing, and the obliquity and precession cycle signals are also clearly expressed in the MGS record (Li et al., 2015). The broken and dotted lines linking Fig. 3a and b indicate peaks and troughs in dust activity and MGS, respectively. As documented by geological records and indicated by the transient simulation, the climate and dust signals in the studied region during the last 150 kyr are overwhelmingly at the precessional frequency. Therefore, for simplicity, we term the combined orbital parameters as precession. Due to the low resolution of loess samples together with chronological errors, the MGS would not be expected to correlate precisely with the simulated dust flux. In general, the MGS correlates with the strength of the East Asian winter wind, with several lags or leads with respect to spring insolation (Liu and Shi, 2009).

Of the total amount of dust emitted in NC and then injected into the atmosphere, about 30% settles in the dust source area, 20% is transported to inland China, and the remaining 50% is subject to long-distance transport to South Korea, Japan, the Pacific, and even to the United States, Canada, Greenland, and elsewhere (Zhang et al., 1997,

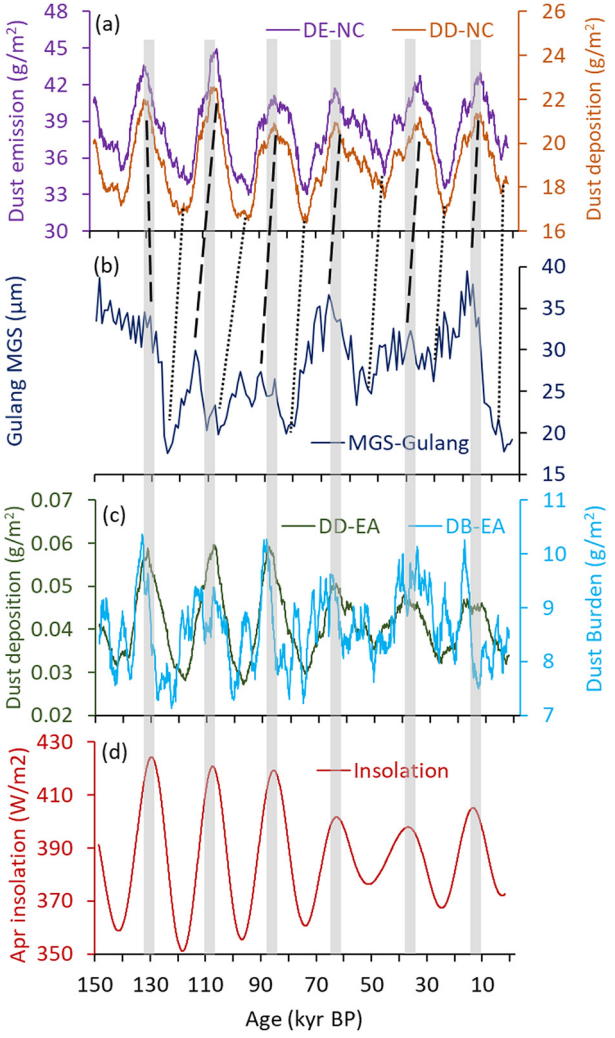

Fig. 3. Time series of dust activities and geological records spanning the last 150 kyr. (a) Simulated spring dust emission flux (DE-NC) and deposition flux (DD-NC) in NC; (b) geological record of the mean grain size (MGS) of loess from Gulang in the Chinese Loess Plateau (CLP); (c) simulated spring dust deposition flux (DD-EA) and column burden (DB-EA) in EA; (d) April insolation at 45°N. The dashed and dotted lines linking (a) and (b) indicate peaks and troughs of dust activity and corresponding MGS, respectively. The six vertical gray-shaded bars represent six HI stages, same as below.

2003; Chen et al., 2017). Like the dust activity in NC, the dust deposition flux (DD-EA) and column burden (DB-EA) for East Asia (EA, 90–115°E, 20–30°N) exhibit an obvious quasi-20-kyr period (Fig. 3c), and the DD-EA cycle co-varies with insolation, with near-perfect timing of the peaks and troughs. The DB-EA is consistent with that of the DD-EA, and it co-varies synchronously with NH spring insolation. However, the DB-EA series also exhibits suborbital- or millennium-scale cyclicity when the insolation gradually increases from low to high. The phasing discrepancy at some periods may be the result of other factors such as internal feedback or variability of the climate system.

The perfect match in periodicity between dust activity, geological records, and insolation, as well as the overwhelming dominance of 20-kyr precession-scale variability, strongly suggest that insolation is the major external driver of the NC dust cycle.

3.2. The Westerly Jet and heating of the TP

Driven thermally by insolation and dynamically by transient eddies, during winter the upper westerly strengthens and expands to the southern margin of the TP, whereas during summer it weakens and withdraws to the north of the TP (Schiemann et al., 2009). The variation of the strength and latitudinal migration of the Westerly Jet directly influence the atmospheric circulation and Asian dust cycle during the spring-summer seasonal transition period (Zhang et al., 1997). The variation of the Westerly Jet may be related to the surface heating of the TP (Krishnamurti, 2010). From an analysis of NCEP reanalysis data, Li and Liu (2015b) found that when the TP is warmer near surface, the Westerly Jet in the upper troposphere weakens to the south of the TP and its axis shifts northward. Throughout the entire simulation period, the sWJ and nWJ were out phase with each other; this means that the sWJ and insolation were in opposite phase, while the nWJ and insolation were in the same phase (Fig. 4a). The inverse phase relationship between the sWJ and nWJ on the precessional scale may be closely related to the thermal heating of the elevated surface of the TP.

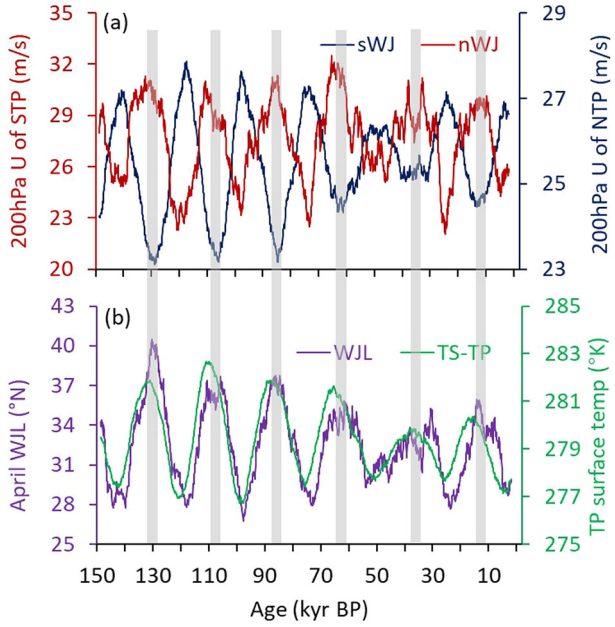

Fig. 4. Simulated time series of 200 hPa zonal wind (a) over north and south of the TP (nWJ and sWJ, respectively), latitudinal location of the Westerly Jet (WJL, defined as the position of the maximum 200 hPa zonal wind at each longitude) in April, and spring surface temperature over the TP (b) during the last 150 kyr.

The role of upper tropospheric circulation in the region is complex, partly because of the high terrain of the TP together with the diversity of the land use of East Asia. Variations in the intensity and shifts in the location of axis of the Westerly Jet are affected by mechanical and thermal forcing of the TP. Time series of the upper tropospheric Westerly Jet axis in April and spring surface temperature over the TP from the long-term transient simulation are presented in Fig. 4b. Similar to the previous research results (Li et al., 2013), the evolution of the axial position of the Westerly Jet during the past 150 kyr exhibits a quasi-20 kyr cycle, which is synchronized with spring surface temperature variations over the TP. Consistent with the finding of Li and Liu (2015b), the sWJ weakens and the nWJ enhanced when spring TP heating is strong. The enhancement of the heating of the surface of TP, caused by increasing NH insolation, modulates the changes in the position of the Westerly Jet with respect to the TP. Solar radiation, as the principal driver of global climate change at the orbital scale, via convection, causes a temperature anomaly aloft during the seasonal transition. The difference in the 200 hPa temperature between May and March (not shown) shows that, influenced by anomalous heating of the TP surface during the HI stage, the upper tropospheric temperature in May increase relative to March, which consequently shifts the axis of the Westerly Jet northward.

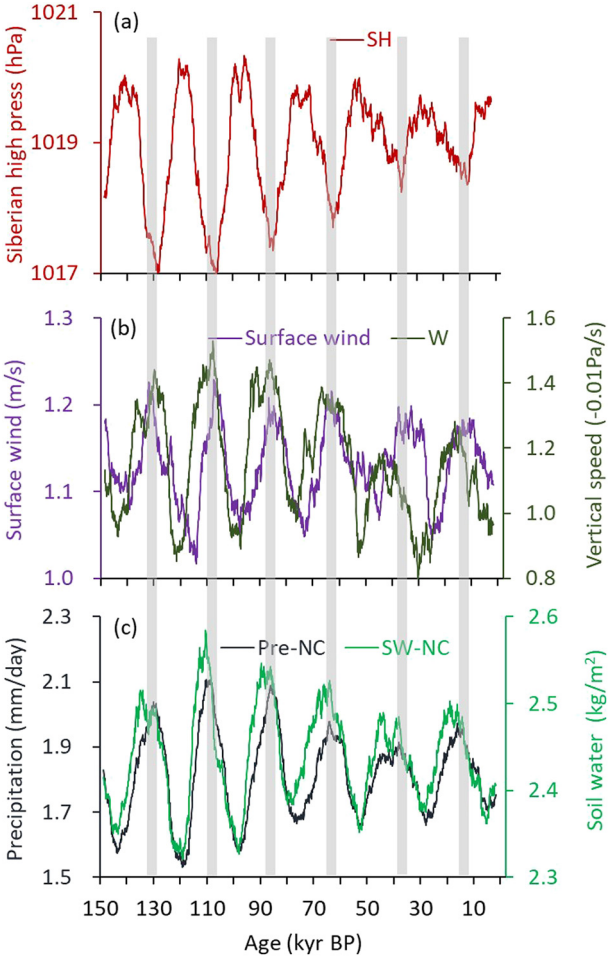

Fig. 5. Simulated time series of relevant climatic elements in dust source area. (a) SH; (b) surface wind and vertical speed (W); (c) precipitation (Pre-NC) and soil water content (SW-NC).

3.3. Surface wind and other relevant climatic elements

The SH is a persistent and dominating high-pressure system in NH during wintertime, which results in a very stable air mass and inhibits interactions between the surface and middle and upper troposphere over the Asian dust source regions. However, in spring, the breakdown of the SH and resulting vertical instability of the atmosphere causes the upper-level waves propagated by the westerly to readily interact with the surface to promote cyclone development (Roe, 2009; Li and Liu, 2015a). In this sense, the spring dust storms are closely related to surface winds (Fig. 5a and b), rather than exclusively with the north-westerly winter monsoon associated with SH (Roe, 2009). Analyses of numerical simulations and observation of dust events in NC indicate that the westerly can affect dust discharge and transport by facilitating the downward transfer of westerly momentum to the near-surface (Seino et al., 2005; Wang et al., 2008a, 2008b; Duan et al., 2013; Han et al., 2019), which intensifies dust activity in spring when the SH weakens. As a key factor for dust activity, the surface wind speed ($\sqrt{(U^2 + V^2)}$) in the dust source area is also in phase with insolation (Fig. 5b). The northward shift, strengthening, and downward propagation of momentum of the Westerly Jet over the TP, and strengthening of northly wind caused by the weakening of the SH and surface warming, result in the greater interaction of the upper tropospheric westerly with the lower surface wind to produce cyclones in dust source areas. With the increased of atmospheric instability during HI stages, the vertical speed (Fig. 5b) is also enhanced and promotes the transfer of dust to the upper layer.

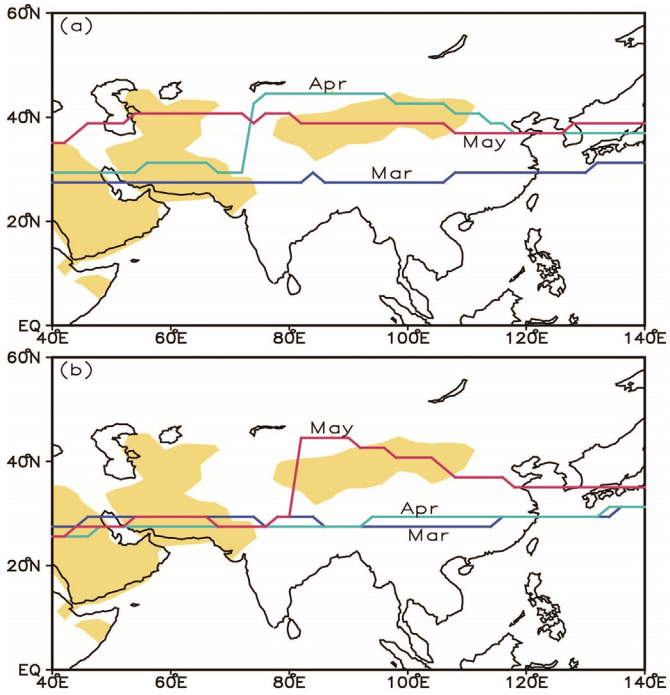

Fig. 6. The latitudinal location of the Westerly Jet axis from March to May in the HI (a) and LI(b) stages. The yellow shaded areas indicate the modern desert regions in CESM1.2 as in Fig. 1. (For interpretation of the references to colour in this figure legend, the reader is referred to the web version of this article.)

As well as the surface wind, precipitation (Pre-NC) and soil water content (SW-NC) over Asian dust source areas also affect dust emission. The spring precipitation and soil water content in NC during the last 150 kyr also exhibit a quasi-20-kyr cycle and change synchronously with spring insolation (Fig. 5c). Pre-NC and SW-NC values are both large when insolation is high, and vice versa. This appears counter-intuitive as moderate-excessive precipitation and wetness would be expected to inhibit dust emission. In other words, precipitation and soil water content are negatively correlated with dust activity on shorter (seasonal, interannual or interdecadal) timescale (Liu et al., 2004). On the orbital scale, Pre-NC and SW-NC within the first 10-cm of soil layer vary slightly from 1.52 to 2.29 mm/day and from 2.32 to 2.58 kg/m^2, respectively (Fig. 5c). In comparison, surface wind can vary by 40%, thus offsetting the inhibitory effect of precipitation and soil water on dust activity. Thus, wind is more important in triggering dust storm outbreaks (Kim et al., 2017) and is considered to be the main driver in dust concentration predictions (Lu and Shao, 2001; Yin et al., 2005). A calculated drought index based on observation station data during 1960–2005 shows that an obvious dryness/wetness trend in NC is absent, although precipitation exhibits a significantly increasing trend (Wang and Tao, 2008). Furthermore, the dependence of dust saltation (emission) on soil moisture is complex: when the surface is very dry (relative humility $<$ 25%) dust emission can even increase with increased soil wetness. This increasing dust emission with wetness could be due to the weakening of interparticle cohesion as water starts to be adsorbed to dry particles (Csavina et al., 2014). Although precipitation can scavenge dust via wet deposition, its effects can occur only during rainfall events that are quite rare in the region.

4. Precessional-scale dynamic mechanism of dust activity

4.1. Shift of the WJ

The monthly variations of the axis of the Westerly Jet from March to May show that during the HI stage the April and May Westerly Jet axes

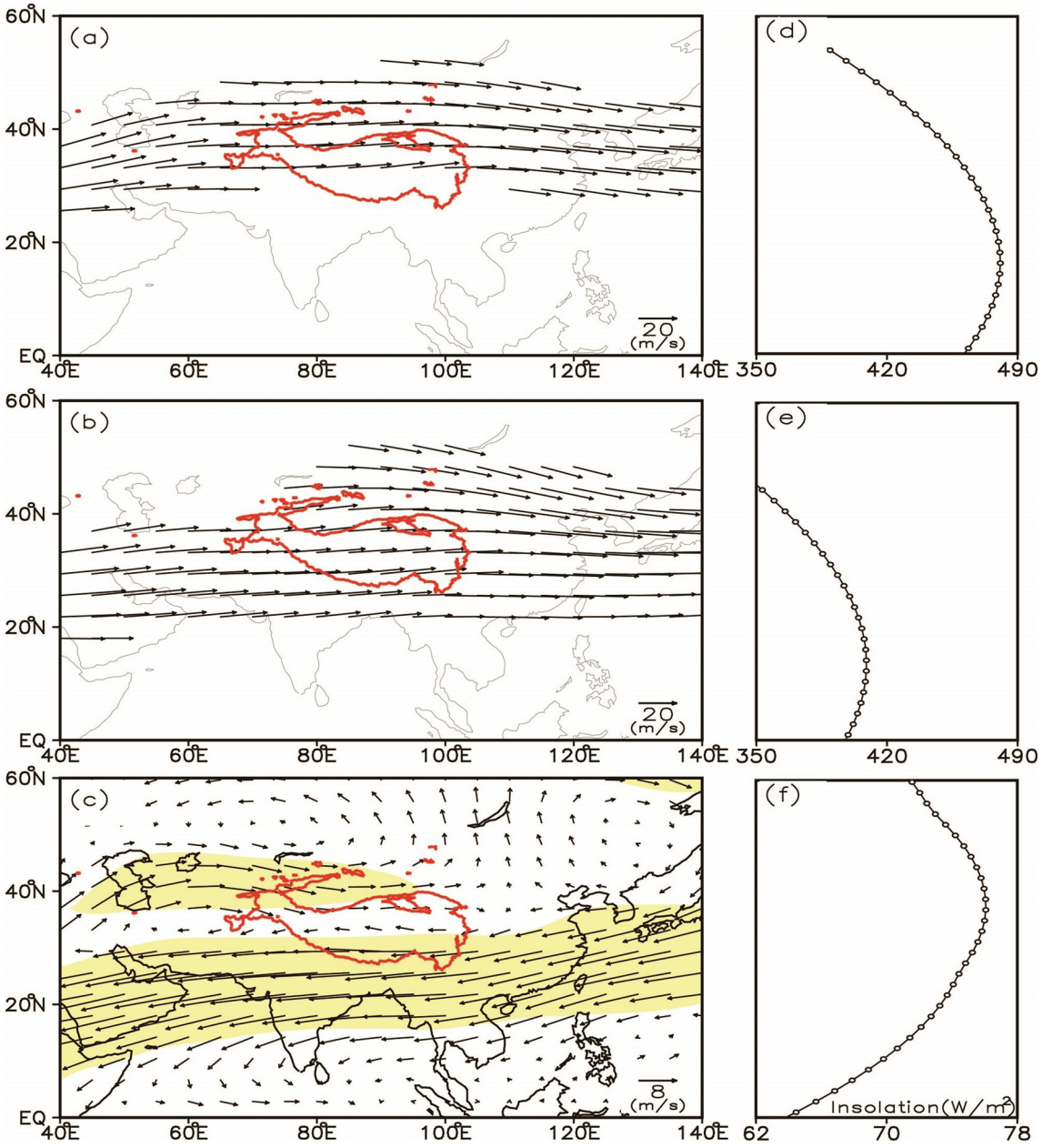

Fig. 7. The April–May 200 hPa wind (m/s) in HI (a), LI (b), difference between HI and LI (c, HI-LI), and their corresponding insolation (d-f, W/m^2). For clarity, only the wind speeds > 20 m/s are showed in (a) and (b). The yellow shaded areas in (c) represent the 95% significance level. (For interpretation of the references to colour in this figure legend, the reader is referred to the web version of this article.)

migrate to the north side of the TP (Fig. 6). When insolation is low, only the May axis moves to the north of the TP while the axes of March and April remain on the south side of the TP. During the HI stage, the area of the April–May zonal wind speed > 20 m/s extends northward over central Asia and the TP, while the maximum westerly wind is also situates to the north of the TP (Fig. 7). However, during the LI stage, the extent of the area with zonal wind > 20 m/s is wider, and the axis locates to the south of the TP. The difference in the zonal wind between HI and LI stages shows that the zonal wind anomaly reaches peak values (> 4 m/s) to the north of the TP. It is noteworthy that the variation of the East Asian subtropical Westerly Jet (EASWJ) stream is relatively weak above Japan, and the largest negative anomaly (< −10 m/s) occurs on the south side of the TP.

The mechanism of the westerly straddling the TP can be explained by means of a schematic diagram (Fig. 8). Driven by differential meridional radiation without the heating from the TP, the temperature distribution is zonal, as is the mid-latitude westerly wind (Fig. 8a). The heating of the TP induces an anomalous temperature field which intensifies the temperature gradient of the upper troposphere to the north of the TP, leading to a westerly anomaly on north of the TP and an easterly anomaly to south (Fig. 8b). Superimposed on the heating of the TP is the enhanced irradiance during the HI stage which peaks at roughly the same latitude as the TP. This amplified heating induces a negative potential vorticity (PV) center in the upper troposphere over the TP. The combined effect of the astronomically-driven solar radiation (Fig. 7f) and the TP-induced heating cause an enhanced westerly on the north side of the TP and a weakened westerly on the south side (Fig. 8c).

4.2. Vertical circulation associated with dust activity

Viewed from the perspective of the meridional vertical circulation

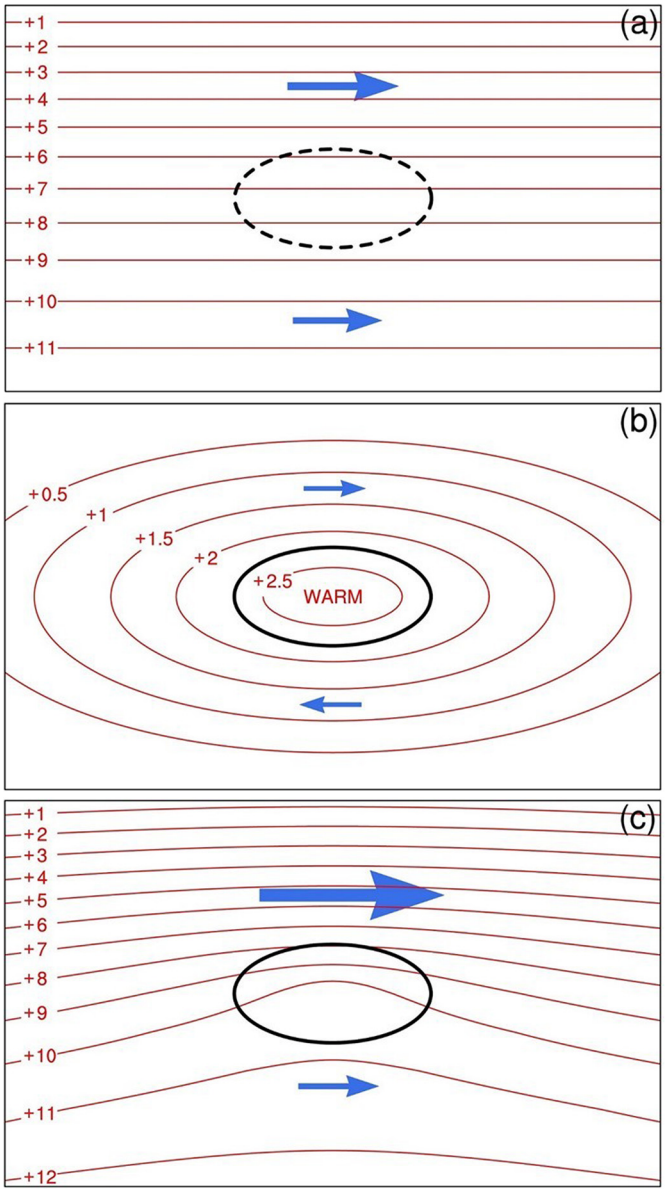

Fig. 8. Schematic diagrams showing ideal distributions of mid-tropospheric temperature (red lines) and upper Westerly Jets (blue arrows) around the TP (black ellipses) in spring, under the influence of orbital-scale solar radiation (a), heating from the TP (b), and the superposition of solar radiation and heating from the TP (c). The red numbers (+1, +2, …) represent the relative temperature values, and WARM indicates the TP heating area. (For interpretation of the references to colour in this figure legend, the reader is referred to the web version of this article.)

field (Fig. 9), in the HI stage, the positive zonal wind anomaly present to the north of the TP appears during the transitional period from spring to summer. The strengthening westerly wind causes the entire upper troposphere to extend down to surface where frequent sandstorms occur (Fig. 9a). Affected by the elevated heat source of the TP, a spring temperature anomaly dipole in the upper troposphere straddles the TP, with positive values to the north (Fig. 9b). In spring, the TP is one of the world's most powerful radiative heat sources (Zhao and Chen, 2001; Wu et al., 2012). The strong heating during the HI stage weakens the sWJ and strengthens the nWJ over the TP, causing the Westerly Jet to shift northward to the north of the TP (Li and Liu, 2015b). Thus, the anomalous radiative warming over the TP is the main reason for the northward position of the WJ.

The average Westerly Jet axis in April in the HI stage moves to the north of the NC desert region, which has important implications for jet stream dynamics. The latitudinal position of the jet axis is crucial in the four-quadrant convergence/divergence (i.e., sinking/rising motion below) of jet stream dynamics (Bluestein, 1993). When mean position of jet axis is shifted to the north of the desert source region, it is likely that the nWJ-associated upward branch (Fig. 9b) of the traverse circulation induced by upper-troposphere divergence/convergence is over the Taklimakan desert, given the large variability of the position of the WJ.

Comparison of the differences of spring sea-level pressure (SLP) and surface temperature field between the HI and LI stages (Fig. 9c) reveals that SLP is significantly reduced, which makes the atmospheric boundary layer unstable. At the same time, the surface warming in the dust source area is significantly higher than in the surrounding area, and its temperature gradient causes the northerly wind to increase over the entire dust emission domain. The percentage change in wind speed ($\sqrt{(U^2 + V^2)}$) for the HI stage relative to the LI stages increases significantly on the northern side of the TP, especially in the dust source area where the increase surface wind speed reaches 40% (Fig. 9). Over the dust source regions, the wind speed increases by > 0.6 m/s; the local maximum reaches 0.8 m/s over the desert source area (Fig. 9d). Given light winds near the ground surface, this 0.6–0.8 m/s difference represents a 30–40% increase (see also Fig. 9a). This is mainly due to the weakening of SH in spring, resulting in an increase in vertical atmospheric instability, and this phenomenon has been strengthened during HI stage as illustrated in Fig. 5b at the precessional scale. SH weakening and surface wind strengthening and their higher interaction jointly give rise to unstable in the dust source areas. The surface wind over the source regions is largely westerly or northwesterly (Fig. 9d). The strengthened westerly wind is consistent with enhanced baroclinicity promoted by the N-S temperature gradient. The westerly and northerly wind increases caused by the gradients of surface pressure and temperature are likely required by the vertical motion via mass continuity.

4.3. Relationship between dust cycle dynamics and the upper westerlies based on modern observations

Spring is the main season of sandstorm in the East Asian and the most wavering season in term of the north-south shifting of the WJ. The sequence of spring dust station-hour averaged for 181 sandstorm stations in NC during 1954–2007 is shown in Fig. 10a. The frequency of spring sandstorm has weakened during the 54 years, which is consistent with the previous research (Zhou and Zhang, 2003). On the inter-decadal scale, however, the dust frequency was high in the 1960s, and then it started to weaken from early 1970s till mid-1990s before slightly rising afterwards.

According to the foregoing analysis, the upper-level westerly wind is a key factor for dust activity on the precessional scale. There is a significant positive correlation (Fig. 10a) between the April WJL and the spring dust sandstorm series based on NCEP reanalysis and observed dust station-hour data in NC during 1954–2007. When sandstorms were more frequent - in the 1960s, at the end of the 20th century, and in the early 21st century (Zhou and Zhang, 2003) - the WJL remained north of ~40°N; otherwise it was south of about 30°N. The correlation coefficient for two sequences is 0.372 (significant at the 99% level). However, correlation coefficients for the relationship between the WJL and the sandstorm frequency in March and May, respectively, are only −0.009 and 0.098 (not significant). This may be because the position of the March WJL remains stable on the south side of the TP, whereas the position of the May WJL is relatively stable on the north side. The April WJL is the most vibrant in the latitudinal wavering. The standard deviations of the WJL in March, April and May are 4.26, 8.08 and 7.13°, respectively. The red, green and purple solid lines in Fig. 10b represent the maximum (average of 1964, 1969 and 1997), minimum (average of

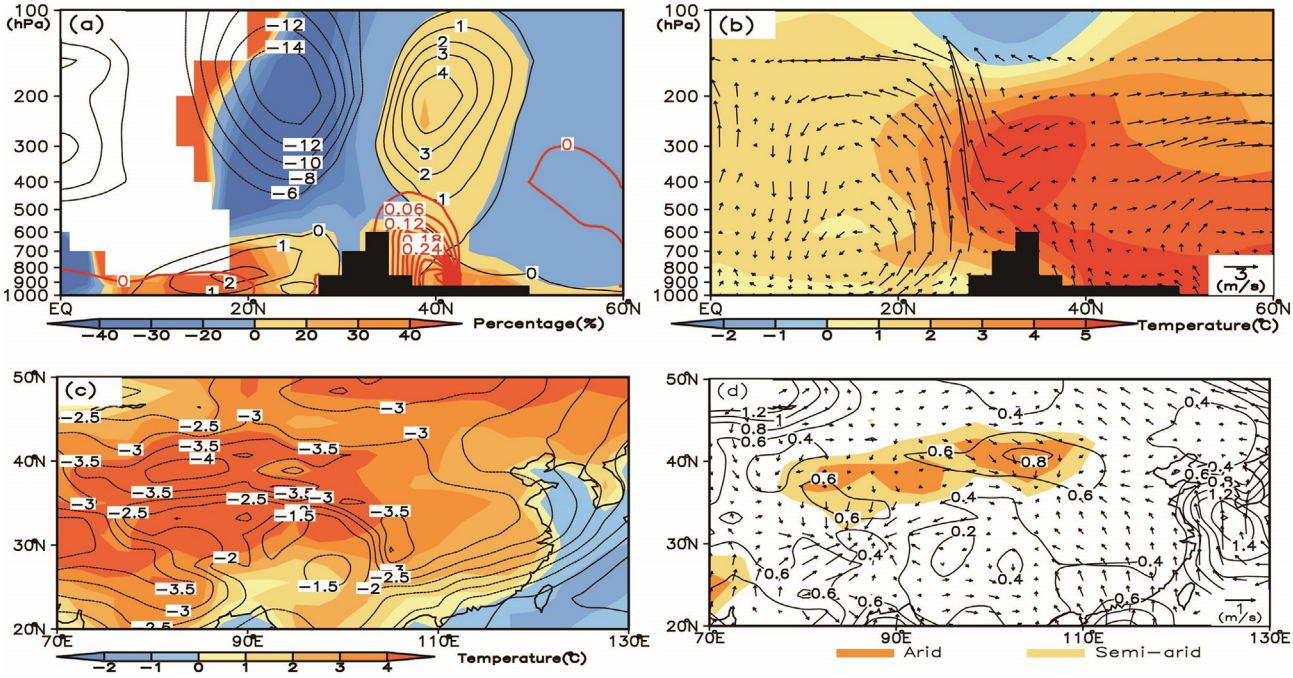

Fig. 9. Differences in circulation fields along the meridional cross-section (averaged over 80–100°E) between the HI and LI stages. (a) The zonal wind (black contour, m/s) and its percentage (shading, %) and dust mass concentration (red contour, mg/kg); (b) the atmospheric temperature (shading, °C) and vertical circulation (vector, the units are m/s for meridional velocity and − 0.01 Pa/s for the vertical pressure velocity); (c) sea-level pressure (shading, SLP, hPa) and surface temperature (black contours, °C); (d) surface wind at σ = 0.95. The yellow and orange shading represents the semi-arid and arid dust source areas consistent with Fig. 1. The black shaded regions in (a) and (b) denote the model topography in the transient experiment. (For interpretation of the references to colour in this figure legend, the reader is referred to the web version of this article.)

1972, 1973 and 1997) and average (average of 1954–2007) of WJL during the 1954–2007. The northernmost part of the WJL is just above the dust source areas. In spring, the variation of zonal wind intensity on the north side of the TP has a strong influence on the frequency of the underlying sandstorm in NC. The stronger westerly winds and the more northward the Westerly Jet axis, the stronger and more frequent dust activities.

The spatial distribution of the correlation coefficients between spring sandstorm frequency in NC and surface temperature in the TP as a whole and the 200 hPa zonal wind speed during the 1954–2007 are plotted in Fig. 10b and c, respectively. Of notable is that a zonally elongated strip of positive correlation ($r > 0.4$, significant at the 99% level) occurs along the northern flank of the TP. This means that a warmer TP is more conducive to the enhancement of the westerly wind on the north side of the TP, which leads to a strengthening of dust activity in NC.

5. Discussion

Notably, in arid and semi-arid desert areas, changes in spring precipitation and soil water content are in-phase with dust activity and inhibit dust emission, which is inconsistent with the modern observation results. We speculate that precipitation and soil water have a weak influence on dust activity on precessional scale, while other factors (e.g. surface wind, temperature, the Westerly Jet) play decisive roles. Modern instrumental observations and reanalysis data show that the sandstorm frequency in NC is positively (negatively) correlated with nWJ (sWJ) strength ($r > 0.4$, significant at the 99% level) from 1954 to 2007, which emphasizes their close relationship; however, precipitation, soil moisture, and vegetation coverage have important effects on short time scales (e.g. seasonal, annual, decadal).

Atmospheric greenhouse gases concentration, surface vegetation coverage, and high latitude ice sheets also influence the upper westerly and dust activity, especially during glacial period (Li et al., 2018; Yu et al., 2019). Geological records show that there are multiple fluctuations (expansion or shrinkage) in dust source areas during the past (Lu et al., 2013). The surface soil erosion status and drought in arid and semiarid dust source area would affect the dust emission, transport, and deposition on multiple spatial and temporal scales. However, the long-term continuous transient experiment described herein only considers insolation change caused by Earth orbital parameters. Essentially, the present simulation can be regarded as a sensitivity study related to insolation on the precessional scale, rather than attempt to accurately reproduce actual dust processes; therefore, we have only made a qualitative comparison of the simulated dust cycles with geological records. Based on modern observations and numerical simulations, Chen et al. (2017) found dust emissions differences between two sub-regions (Taklimankan and Gobi deserts), and the orbital scale changes deserve further study. In addition, owing to the coarse resolution and inaccurate age of the long records of loess deposits, speleothems, and marine deposits from East Asia, it is difficult to distinguish the seasonal variability. As proposed by Serno et al. (2017), the orbital-scale dust cycle could be the result of the expansion of dust activity from spring to summer, which will need to be investigated in the future research using simulations and high-resolution geological records.

6. Conclusions

Using the latest version of the NCAR CESM, and based on the orbital acceleration technique, including the atmosphere, land, ocean, ice and their coupled processes, we analyzed the orbital-scale characteristics of dust activity and relevant climatic elements, examined the possible modulation of the upper Westerly Jet, and explored the possible mechanism governing interplays of insolation, the Westerly Jet and the dust cycle. The principal results are as follows: In the long-term transient simulation, there is a dominant 20-kyr precessional cyclicity in dust emission, sediment flux, and air column concentrations in spring over northern China during the last 150 kyr. Dust activity is in near-

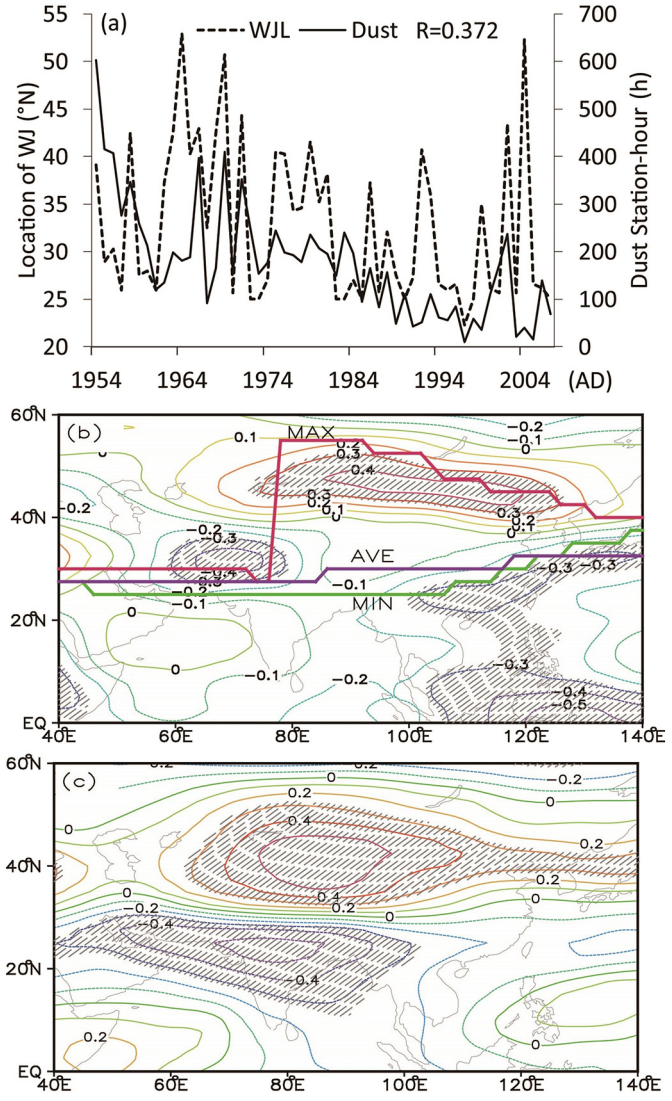

Fig. 10. Correlations between the sandstorm frequency in spring in NC and 200 hPa WJL in April during 1954–2007. (a) Year-to-year variations of the sandstorm frequency and the WJL; (b) distribution of correlation coefficients of the 200 hPa zonal winds at each grid cells with the sandstorm frequency; (c) same as (b), but with the TP surface temperature. The red, green and purple solid lines in (b) indicate the maximum, minimum and average positions of the WJL during 1954–2007, respectively. The hatched areas represent the 95% significance level in (a) and (b). (For interpretation of the references to colour in this figure legend, the reader is referred to the web version of this article.)

perfect synchrony with April insolation at 45°N. During the high-insolation stage, the weakening of the Siberian high in spring and the anomalous temperature gradient produce cyclogenesis which intensifies dust activity in the desert regions. In addition, the elevated heating over the TP modulates the latitudinal swings of the Westerly Jet and thus influences the vertical circulation and dust activity. The strengthening of the upper westerly, combined with weakening of the Siberian high and surface warming, eventually lead to an increase in surface wind ($\sqrt{(U^2 + V^2)}$) by up to 40% in the high-insolation stage, giving rise to atmospheric instability which promotes dust activity over the dust source regions.

Declaration of competing interest

The authors declared that they have no conflicts of interest to this work.

We declare that we do not have any commercial or associative interest that represents a conflict of interest in connection with the work submitted.

Acknowledgments

This work was jointly supported by the Strategic Priority Research Program of Chinese Academy of Sciences (XDA20070103, XDB26000000), the National Natural Science Foundation of China (41690115) and the National Key Research and Development Program of China (2016YFA0601904). The authors would like to thank Xiaoxun Xie for drawing Fig. 8, Dr. Jan Blomendal for language editing, and two anonymous reviewers for their constructive comments. Xinzhou Li is the support of the Belt and Road Center for Climate and Environment Studies, Institute of Earth Environment, Chinese Academy of Sciences. The modeling data used in this study are achieved on the East Asian Paleoenvironmental Science Database (http://paleodata.ieecas.cn). The observational data of sandstorms were obtained from the China Meteorological Information Center (http://data.cma.cn). The NCEP reanalysis data were downloaded from this website (https://www.esrl.noaa.gov). The dust data were provided by the Multi-angle Imaging Spectro-radiometer (MISR, http://www-misr.jpl.nasa.gov).

References

Anderson, P.M., Barnosky, C.W., Bartlein, P.J., Behling, P.J., Brubaker, L., Cushing, E.J., 1988. Climatic changes of the last 18,000 years: observations and model simulations. Science 241 (4869), 1043.

Bar-matthews, M., Ayalon, A., Gilmour, M., Matthewsh, A., Hawkesworth, C.J., 2003. Sea-land oxygen isotopic relationships from planktonic foraminifera and speleothems in the Eastern Mediterranean region and their implication for paleorainfall during interglacial intervals. Geochim. Cosmochim. Ac. 67 (17), 3181–3199.

Bluestein, H.B., 1993. Synoptic-Dynamic Meteorology in Midlatitudes. Vol. II: Observations and Theory of Weather Systems. Oxford University Press (594 pp).

Buchard, V., Randles, C.A., Da Silva, A.M., Darmenov, A., Colarco, P.R., Govindaraju, R., Ferrare, R., Hair, J., Beyersdorf, A.J., Ziemba, L.D., Yu, H., 2017. The MERRA-2 aerosol reanalysis, 1980 onward. Part II: Evaluation and case studies. J. Clim. 30 (17), 6851–6872.

Chang, E.K., Lee, M.S., Swanson, K.L., 2002. Storm track dynamics. J. Clim. 15, 2163–2183.

Chen, S.Y., Huang, J.P., Li, J.X., Jia, R., Jiang, N.X., Kang, L.T., Ma, X.J., Xie, T.T., 2017. Comparison of dust emissions, transport, and deposition between the Taklimakan Desert and Gobi Desert from 2007 to 2011. Sci. China Earth Sci. 60, 1338–1355.

Cheng, H., Zhang, P.Z., Spotl, C., Edwards, R.L., Cai, Y.J., Zhang, D.Z., Sang, W.C., Tan, M., An, Z.S., 2012. The climatic cyclicity in semiarid-arid central Asia over the past 500,000 years. Geophys. Res. Lett. 39, 1–5.

Chiang, J.C., Fung, I.Y., Wu, C.H., Cai, Y., Edman, J.P., Liu, Y., Day, J.A., Bhattacharya, T., Mondal, Y., Labrousse, C.A., 2015. Role of seasonal transitions and Westerly Jets in East Asian paleoclimate. Quaternary Sci. Rev. 108, 111–129.

Csavina, J., Field, J., Félix, O., Corral-Avitia, A.Y., Sáez, A.E., Betterton, E.A., 2014. Effect of wind speed and relative humidity on atmospheric dust concentrations in semi-arid climates. Sci. Total Environ. 487, 82–90.

Ding, Z.L., Ranov, V., Yang, S.L., Finaev, A., Han, J.M., Wang, G.A., 2002. The loess record in southern Tajikistan and correlation with Chinese loess. Earth Planet Sc. Lett. 200 (3–4), 387–400.

Duan, H.X., Li, Y.H., Pu, Z.X., Zhao, J.H., Zhang, L., 2013. The influence of high level jet on dust transportation in a sandstorm process. Chinese with English abstract. J. Desert Res. 33 (5), 1461–1472.

Gelaro, R., McCarty, W., Suárez, M.J., Todling, R., Molod, A., Takacs, L., Wargan, K., 2017. The modern-era retrospective analysis for research and applications, version 2 (MERRA-2). J. Clim. 30 (14), 5419–5454.

Han, W.X., Fang, X.M., Ye, C.C., Teng, X.H., Zhang, T., 2014. Tibet forcing Quaternary stepwise enhancement of Westerly Jet and central Asian aridification: carbonate isotope records from deep drilling in the Qaidam salt playa, NE Tibet. Glob. Planet. Chang. 116, 68–75.

Han, W.X., Lü, S., Appel, E., Berger, A., Madsen, D., Vandenberghe, J., Yu, L.P., Han, Y.X., Yang, Y.B., Zhang, T., Teng, X., Fang, X.M., 2019. Dust storm outbreak in central Asia after ~3.5 kyr BP. Geophys. Res. Lett. 46, 7624–7633.

Hurrell, J.W., Holland, M.M., Gent, P.R., Ghan, S., Kay, J.E., Kushner, P.J., Lipscomb, W.H., 2013. The Community Earth System Model: a framework for collaborative research. B. Am. Meteorol. Soc. 94 (9), 1339–1360.

Jackson, C.S., Broccoli, A.J., 2003. Orbital forcing of Arctic climate: mechanisms of climate response and implications for continental glaciations. Clim. Dynam. 21, 539–557.

Jia, J., Liu, H., Gao, F., Xia, D., 2018. Variations in the westerlies in Central Asia since 16 ka recorded by a loess section from the Tien Shan Mountains. Palaeogeo. Palaeoclim. Palaeoecol. 504, 156–161.

Kalnay, E., Kanamitsu, M., Kistler, R., Collins, W., Deaven, D., Gandin, L., ... Zhu, Y.,

1996. The NCEP/NCAR 40-year reanalysis project. B. Am. Meteorol. Soc. 77 (3), 437–471.
Kim, H., Zohaib, M., Cho, E., Kerr, Y.H., Choi, M., 2017. Development and assessment of the sand dust prediction model by utilizing microwave-based satellite soil moisture and reanalysis datasets in East Asian desert areas. Adv. Meteorol. 2017, 1917372. https://doi.org/10.1155/2017/1917372.
Kohfeld, K.E., Graham, R.M., De Boer, A.M., Sime, L.C., Wolff, E.W., Le Quéré, C., Bopp, L., 2013. Southern Hemisphere westerly wind changes during the Last Glacial Maximum: paleo-data synthesis. Quaternary Sci. Rev. 68, 76–95.
Krishnamurti, T.N., 2010. The subtropical jet stream of winter. J. Atmos. Sci. 18 (18), 172–191.
Kutzbach, J.E., 1981. Monsoon climate of the early Holocene: climate experiment with the Earth's orbital parameters for 9000 years ago. Science 214, 59–61.
Kutzbach, J.E., Liu, X.D., Liu, Z.Y., Chen, G.S., 2008. Simulation of the evolutionary response of global summer monsoons to orbital forcing over the past 280,000 years. Clim. Dynam. 30, 567–579.
Li, X., Liu, X.D., 2015a. Relation of spring dust-storm activities in northern China and changes of upper westerlies. Plateau Meteorol 34 (5), 1292–1300 (in Chinese with English abstract).
Li, X.Z., Liu, X.D., 2015b. Numerical simulation of Tibetan Plateau heating anomaly influence on Westerly Jet in spring. J. Earth Sys. Sci. 124 (8), 1599–1607.
Li, X.Z., Liu, X.D., Qiu, L.J., An, Z.S., Yin, Z.Y., 2013. Transient simulation of orbital-scale precipitation variation in monsoonal East Asia and arid central Asia during the last 150 ka. J. Geophys. Res. 118, 7481–7488.
Li, Y., Su, N., Liang, L., Ma, L., Yan, Y., Sun, Y., 2015. Multiscale monsoon variability during the last two climatic cycles revealed by spectral signals in Chinese loess and speleothem records. Clim. Past 11, 1067–1075.
Li, X.Z., Pan, Z.T., Liu, X.D., 2016. Numerical simulation of influence of Tibetan Plateau uplift on winter dust cycle in Asian arid regions. Environ. Earth Sci. 75 (7), 1–12.
Li, X.Z., Liu, X.D., Zhao, H.L., 2017. Transient simulation of the Tibetan Plateau modulated distinct orbital-scale precipitation variation in East and South Asia. Palaeogeo. Palaeoclim. Palaeoecol. 485, 899–905.
Li, X., Zhang, R., Zhang, Z., Yan, Q., 2018. What enhanced the aridity in Eocene Asian inland: global cooling or early Tibetan Plateau uplift? Palaeogeo. Palaeoclim. Palaeoecol. 510, 6–14.
Li, Y., Song, Y., Qiang, M., Miao, Y., Zeng, M., 2019. Atmospheric dust variations in the Ili Basin, northwest China during the last glacial period as revealed by a high mountain loess-paleosol sequence. J. Geophys. Res. 124, 8449–8466.
Liu, X.D., Shi, Z.G., 2009. Effect of precession on the Asian summer monsoon evolution: a systematic review. Chin. Sci. Bull. 54, 3720–3730.
Liu, X.D., Yin, Z.Y., Zhang, X.Y., Yang, X.C., 2004. Analyses of the spring dust storm frequency of northern China in relation to antecedent and concurrent wind, precipitation, vegetation, and soil moisture conditions. J. Geophys. Res. 109 (D16), 365–391.
Liu, S.L., Wang, T., Mouat, D., 2013. Temporal and spatial characteristics of dust storms in the Xilingol grassland, northern China, during 1954-2007. Regional Environ. Change. 13, 43–52.
Liu, H., Liu, X., Dong, B., 2018. Influence of Central Siberian Snow-Albedo feedback on the Spring East Asian dust cycle and connection with the preceding winter Arctic oscillation. J. Geophys. Res. 123 (23), 13,368–13,385.
Lorenz, S.J., Lohmann, G., 2004. Acceleration technique for Milankovitch type forcing in a coupled atmosphere-ocean circulation model: method and application for the Holocene. Clim. Dynam. 23, 727–743.
Lu, H., Shao, Y., 2001. Toward quantitative prediction of dust storms: an integrated wind erosion modelling system and its applications. Environ. Model. Softw. 16 (3), 233–249.
Lu, H., Yi, S., Xu, Z., Zhou, Y., Zeng, L., Zhu, F., ... Mason, J., 2013. Chinese deserts and sand fields in Last Glacial Maximum and Holocene Optimum. Chinese Sci. Bull. 58 (23), 2775–2783.
Mahowald, N.M., Muhs, D.R., Levis, S., Rasch, P.J., Yoshioka, M., Zender, C.S., Luo, C., 2006. Change in atmospheric mineral aerosols in response to climate: last glacial period, preindustrial, modern, and doubled carbon dioxide climates. J. Geophys. Res. 111 (D10), 1879–1894.
Nagashima, K., Tada, R., Matsui, H., Irino, T., Tani, A., Toyoda, S., 2007. Orbital-and millennial-scale variations in Asian dust transport path to the Japan Sea. Palaeogeo. Palaeoclim. Palaeoecol. 247 (1–2), 144–161.
Neale, R.B., Chen, C.C., Gettelman, A., Lauritzen, P.H., Park, S., Williamson, D.L., ... Tayor, M.A., 2010. Description of the NCAR Community Atmosphere Model (CAM5.0) NCAR Tech. Note NCAR/TN-486+ STR. (doi:10.1.1.422.3202).
Petit, J.R., Jouzel, J., Raynaud, D., Barkov, N.I., Barnola, J.M., Basile, I., Delmotte, M., 1999. Climate and atmospheric history of the past 420,000 years from the Vostok ice core, Antarctica. Nature 399, 429–436.
Pinot, S., Ramstein, G., Harrison, S.P., Prentice, I.C., Guiot, J., Stute, M., Joussaume, S., 1999. Tropical paleoclimates at the Last Glacial Maximum: comparison of Paleoclimate Modeling Intercomparison Project (PMIP) simulations and paleodata. Clim. Dyn. 15, 857–875.
Prell, W.L., Kutzbach, J.E., 1987. Monsoon variability over the past 150,000 years. J. Geophys. Res. 92, 8411–8425.
Roe, G., 2009. On the interpretation of Chinese loess as a paleoclimate indicator. Quat. Res. 71, 150–161.
Schiemann, R., Lüthi, D., Schär, C., 2009. Seasonality and interannual variability of the Westerly Jet in the Tibetan Plateau region. J. Clim. 22, 2940–2957.
Seino, N., Sasaki, H., Yamamoto, A., Mikami, M., 2005. Numerical simulation of mesoscale circulations in the Tarim Basin associated with dust events. J. Meteorol. Soc. Jpn. 83A, 205–218.
Serno, S., Winckler, G., Anderson, R.F., Jaccard, S.L., Kienast, S.S., Haug, G.H., 2017. Change in dust seasonality as the primary driver for orbital-scale dust storm variability in East Asia. Geophys. Res. Lett. 44 (8), 3796–3805.
Sun, D.H., 2004. Monsoon and westerly circulation changes recorded in the late Cenozoic Aeolian sequences of Northern China. Glob. Planet. Chang. 41 (1), 63–80.
Sun, Y., Kutzbach, J., An, Z., Clemens, S., Liu, Z., Liu, W., ... Yan, Y., 2015. Astronomical and glacial forcing of East Asian summer monsoon variability. Quaternary Sci. Rev. 115, 132–142.
Uno, I., Eguchi, K., Yumimoto, K., Takemura, T., Shimizu, A., Uematsu, M., ... Sugimoto, N., 2009. Asian dust transported one full circuit around the globe. Nat. Geosci. 2, 557–560.
Wang, J.S., Tao, J.H., 2008. Tendency of dryness/wetness over Northwest China in recent 50 years. IEEE International Geoscience and Remote Sensing Symposium 4 (IV), 962–965.
Wang, P., Clemens, S., Beaufort, L., Braconnot, P., Ganssen, G., Jian, Z., ... Sarnthein, M., 2005. Evolution and variability of the Asian monsoon system: state of the art and outstanding issues. Quaternary Sci. Rev. 24, 595–629.
Wang, Y., Cheng, H., Edwards, R.L., Kong, X., Shao, X., Chen, S., ... An, Z., 2008a. Millennial- and orbital-scale changes in the East Asian monsoon over the past 224,000 years. Nature 451, 1090–1093.
Wang, M.Z., Wei, W.S., Yang, L.M., Li, Y.H., Xiao, S.J., Aili, M., 2008b. Analysis on circulation dynamical structure of a strong sand-dust storm case from east in Tarim Basin. Chinese with English abstract. J. Desert Res. 28 (2), 370–376.
Wang, Y., Jian, Z.M., Zhao, P., Xiao, D., Chen, J.M., 2016. Relative roles of land- and ocean atmosphere interactions in Asian-Pacific thermal contrast variability at the precessional band. Sci. Rep. 6, 28349.
Wu, G.X., Liu, Y.M., He, B., Bao, Q., Duan, A.M., Jin, F.F., 2012. Thermal controls on the Asian summer monsoon. Sci. Rep. 2, 404.
Yin, D., Nickovic, S., Barbaris, B., Chandy, B., Sprigg, W.A., 2005. Modeling wind-blown desert dust in the southwestern United States for public health warning: a case study. Atmos. Environ. 39 (33), 6243–6254.
Yoshioka, M., Mahowald, N., Conley, A., Collins, W., Fillmore, D., Coleman, D., 2007. Impact of desert dust radiative forcing on Sahel precipitation: relative importance of dust compared to sea surface temperature variations, vegetation changes and greenhouse gas warming. J. Clim. 20, 1445–1467.
Yu, K., Lehmkuhl, F., Schlütz, F., Diekmann, B., Mischke, S., Grunert, J., ... G Zeeden, C., 2019. Late Quaternary environments in the Gobi Desert of Mongolia: vegetation, hydrological, and palaeoclimate evolution. Palaeogeo. Palaeoclim. Palaeoecol. 514, 77–91.
Yuan, D., Cheng, H., Edwards, R.L., Dykoski, C.A., Kelly, M.J., Zhang, M., ... Dorale, J.A., 2004. Timing, duration, and transitions of the last interglacial Asian monsoon. Science 304, 575–578.
Zender, C.S., Bian, H., Newman, D., 2003. Mineral Dust Entrainment and Deposition (DEAD) model: description and 1990s dust climatology. J. Geophys. Res. 108 (D14), 4416.
Zhang, X.Y., Arimoto, R., An, Z.S., 1997. Dust emission from Chinese desert sources linked to variations in atmospheric circulation. J. Geophys. Res. 102 (23), 28041–28047.
Zhang, X.Y., Gong, S.L., Zhao, T.L., Arimoto, R., Wang, Y.Q., Zhou, Z.J., 2003. Sources of Asian dust and role of climate change versus desertification in Asian dust emission. Geophys. Res. Lett. 30 (24), 5–8.
Zhang, Y.C., Kuang, X.Y., Guo, W.D., Zhou, T.J., 2006. Seasonal evolution of the upper-tropospheric westerly jet core over East Asia. Geophys. Res. Lett. 33, L11708.
Zhang, R., Jiang, D., Zhang, Z., Cheng, Z., Zhang, Q., 2017. Comparison of the climate effects of surface uplifts from the northern Tibetan Plateau, the Tianshan, and the Mongolian Plateau on the East Asian climate. J. Geophys. Res. 122 (15), 7949–7970.
Zhao, P., Chen, L.X., 2001. Climatic features of atmospheric heat source/sink over the Qinghai-Xizang Plateau in 35 years and its relation to rainfall in China. Sci. China Earth Sci. 44 (9), 858–864.
Zhao, T.L., Gong, S.L., Zhang, X.Y., Blanchet, J.P., McKendry, I.G., Zhou, Z.J., 2006. A simulated climatology of Asian dust aerosol and its trans-pacific transport. Part I: mean climate and validation. J. Clim. 19, 88–103.
Zhou, Z., Zhang, G., 2003. Typical severe dust storms in northern China during 1954–2002. Chin. Sci. Bull. 48 (21), 2366–2370.